*Essential Readings in Light Metals: Cast Shop for Aluminum Production.*
Edited by John F. Grandfield and Dmitry G. Eskin.



# ON THE MECHANISM OF SURFACE CRACKING IN DC CAST 7XXX AND 6XXX EXTRUSION INGOT ALLOYS

Steinar Benum, Dag Mortensen, Hallvard Fjær, Hilde-Gunn Øverlie and Oddvin Reiso

Hydro Aluminium a.s., R&D Materials Technology, N-6600 Sunndalsøra, Norway

Institute for Energy Technology, N-2027 Kjeller, Norway

## Abstract

When applying the Hydro variant (Hycast Gas Cushion) of the Showa Denko gas slip technology for casting extrusion ingots of 7xxx alloys surface cracks occasionally occurred. Especially one alloy with 0.3 wt.% Cu caused problems. In order to identify the problem, the casting process for these alloys was simulated by a coupled stress, thermal and fluid flow model (ALSIM/ALSPEN). The simulations were designed as a factorial trial where casting speed, ramping of the speed, casting temperature, cone height of the starting block, cooling water efficiency and primary cooling were systematically varied. The hoop stress in the surface at the temperature when 97.5% of the material was solidified was used as a crack sensitivity indicator. Three stages were identified: (I) At the start a maximum hoop stress evolved, (II) then a minimum stress occurred before (III) the stress reached a stable level. For an AA6060 alloy the stress was found to be zero in the stable stage while the AA7108 alloy experienced tension stress also during the steady state regime. Based on the factorial analysis it was found that the stable stress increased most rapidly with increasing casting speed and decreased with an increased primary cooling and a reduced melt temperature.

Furthermore, the initiation and propagation of cracks were discussed based on investigations on real cracks. Here it was observed that cracks tended to initiate when oxide lumps were released from the hot top. Also, the crack surface was heavily oxidized with an oxide film covering the whole surface. The role of this oxide film for crack propagation is still an issue for debate.

## Introduction

Cracks penetrating the surface section 10 to 50 mm into the ingot are normally not a topic for casting of standard extrusion ingot alloys. For some alloys, especially within the 7xxx segment, Hydro Aluminium has experienced problems with such cracks. Casthouse experience [1] has shown that the frequency of cracks depends on casting speed, metal temperature, cooling water efficiency, starting block design, amount of gas (mixture of Ar and O) used and cooling from the mould wall. Alloys with Cu are the most sensitive alloys for these cracks penetrating the surface in the casting direction. Extrusion ingots with surface cracks are believed to be even more detrimental for the quality of extrusions than center cracks. It is therefore essential to control the formation of such cracks to avoid scrap production in the casthouse.

In the present work the origin of these cracks has been investigated by numerical modelling of the stress and strain state in the surface during the critical last period of solidification and by metallographic observations. An AA7108 alloy with 0.10 wt.%Si, 0.20 wt.%Fe, 0.3 wt.%Cu, 1.25 wt.%Mg, 5.5 wt.%Zn was used as a case study alloy.

## Modelling

### The coupled ALSIM/ALSPEN model

The modelling approach is similar to what was applied in [2]. ALSIM [3] is a finite element method model for the development of the time dependent heat and fluid flows during

DC casting. ALSPEN [4] is a corresponding stress model, solving the compatibility equations, the momentum equations and the constitutive equations. The material is described as an elastic-viscoplastic material. The solution domain is the part of the ingot that is considered to be solid, i.e. where the temperature is predicted to be below a given coherency temperature $T_c$.

These models have been coupled, as explained in [5], and the influence of calculated displacements and pressure on the thermal boundary conditions between the ingot and the bottom block are included in the ALSIM/ALSPEN model. Where the local temperature of the ingot is higher than $T_c$, a heat transfer coefficient depending on the ingot surface temperature is applied for the bottom of the ingot. Where the temperature has become lower than $T_c$, and ALSPEN has computed the displacements, the heat transfer coefficient becomes dependent on both the local gap distance and the estimated contact pressure. Where the calculated gap has a magnitude of more than 0.2 mm, an air gap thermal boundary condition is applied. Where the gap distance is calculated to be less than 0.2 mm, the heat transfer coefficient is assumed to depend on the local surface temperature of the ingot and the normal pressure $p_n$. With ALSPEN, vertical forces, counterbalancing the total weight of the ingot, are distributed underneath the ingot. Emulating some elastic response from the starting block, the local contact pressure $p_n$ is estimated from the calculated gap distance. Although not believed to be accurate, this formulation enables us to incorporate some effect of temperature and pressure dependency in the contact heat transfer. More details about this approach are given in [6].

Cracking tendency parameter

Since starting cracks at the surface propagate in the vertical direction, it is of interest to analyze the stress component in the direction perpendicular to the crack direction. A similar approach was followed in [6] for the case of centre cracks. In that case modelling results were compared with measured crack lengths and it was shown that both the maximum hoop stress and the maximum hoop viscoplastic strain rate at solid fraction of 0.95 correspond very well with a ranking of the hot tearing trials based on observed crack lengths.

As stated in [6]; although in this work the constitutive equation used to describe the rheological behaviour of the material are independent of the mean stress, work done by Martin et al. [7] suggests that the mean stress can also have an effect on the behaviour of the material. Martin et al. consider the mushy zone as a porous metallic material saturated with liquid, and propose constitutive equations for the material behaviour where both the first and second invariant of the stress tensor are introduced. In our case at the surface in the position corresponding to a solid fraction equal to 0.975, the radial stress is zero and the vertical stress component is very small compared to the hoop stress. The mean stress is then approximately equal to one third of the hoop stress, which is the cracking tendency parameter in this study.

## Simulation Experiments

Design of simulations experiments

The simulation experiments were designed by using a full design of experiments (DOE) [8] with 5 parameters, i.e., $2^n = 64$ simulations. Henriksen & al [9] have reported similar use of ALSIM/ALSPEN for a related problem. The method improves and fasten the interpretation of the results of the simulations. Even though computer simulations provide a relatively clear output without any "noise" it might be difficult to investigate really complicated phenomena without such a statistical approach followed by multivariate analyses of the results.

The simulations were based on a Hycast Gas Cushion 203 mm diameter mould. The solidification path and the thermal conductivity for the AA7108 and AA6060 alloys were calculated utilizing the microstructural software Alstruc [10] and the solidification paths are shown in Figure 1. Constitutive laws for the mechanical behavior were based on internal work in Hydro and fitting of the coefficients in a modified Ludwik's law [11].

It was chosen to vary the same parameters as indicated by casthouse experience, i.e., casting speed (V), total casting length for ramping of the speed (L), metal temperature (T), cooling water efficiency, starting block design, amount of gas used and cooling from the mould walls. Four of these parameters, casting speed, metal temperature, starting block design and cooling from mould walls may be directly used as input to ALSIM/ALSPEN. Modifications of the starting block design that are used are shown in Figure.2. One variant with a relatively large cone in the middle and one without were used. The parameter used in the statistical analyses was the cone height (H).

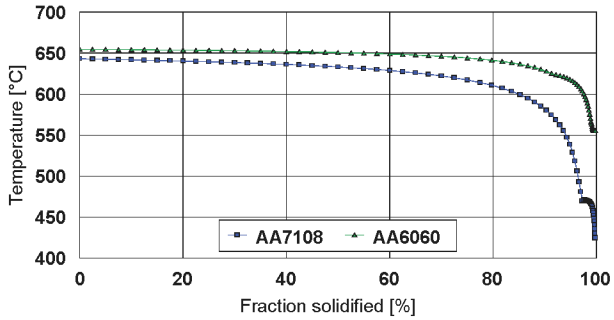


Figure 1: Solidification paths for AA7108 and AA6060.

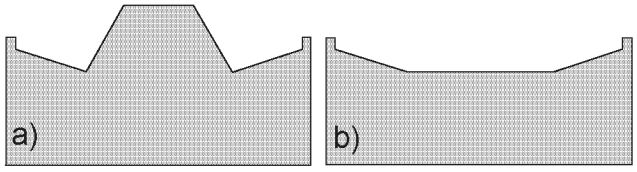


Figure 2: The two cone designs used in the DOE simulations, a) H= 0.044 m, b) H = 0 m.

The effect of the gas flow and the cooling from the mould wall and the water efficiency can not be used as direct input to the model. Instead, it is chosen to use the cooling height (CH) to simulate changes in gas flow or cooling from the mould wall. The water efficiency was simulated by changing the temperature for transition from film boiling to nucleate boiling ($T_F$). The cooling height is known to be somewhat controlled by the gas flow and should give an indication on how the gas flow affects the cracking tendency. In these simulations the cooling height is defined as the distance from the hot top to the water hit point and is varied by varying the height of the mould wall. The transition temperature for film to nucleate boiling varies with water speed, temperature and quality. With a constant water flow applied this would only relate to water quality or

temperature in the present work. The real values of the different parameters are given in Table I together with the coded values used in the multivariate analyses.

Table I The real and coded values for the five parameters varied in the DOE simulations

| Parameter | V [m/s] | L [m] | T [°C] | H [m] | $T_F$ [°C] | CH [m] |
|---|---|---|---|---|---|---|
| Min. real value | 0.00092 | 0.08 | 650 | 0 | 225 | 0.03 |
| Coded value | -1 | -1 | -1 | -1 | -1 | -1 |
| Max. Real Value | 0.00183 | 0.5 | 710 | 0.04 4 | 375 | 0.05 |
| Coded values | 1 | 1 | 1 | 1 | 1 | 1 |

The filling time of the mould was kept constant at 20 seconds in all trials. The initial starting speed in all simulations was 55 mm/min. Ramping of the speed up to stationary casting speed started after 30 mm.

Typical features of hoop stress during casting

The typical behaviour of the Hoop stress at the surface during the initial stage of casting and the steady state regime for the AA7108 alloy is shown in Figure 3 for simulation 1 and 33. In simulation 1 the coded values were all set to 1 and in simulation 33 all coded values were set to 1 except for CH that was set to –1. This means that only the contact area in the primary cooling region were changed. Both figures show a maximum Hoop stress as the first surface reaches the temperature were the solid fraction is 0.975. This stress is further on denoted $\sigma_{max.}$ Then the stress at this point decreases and instead of tensile stress there is compression of the surface, denoted $\sigma_{min.}$ Finally, the stress increases and a stable level of tension, denoted $\sigma_{cont}$, is reached. The oscillations observed are caused by the interpolation of stress values in the finite element mesh. A refinement of the mesh will reduce the oscillations. As can be seen from Figure 3, a reduced primary cooling lowers the maximum tensile stress, decreases the maximum pressure and increases the steady state tensile stress. This could be beneficial with regard to initiation of hot tearing at the very start, but not for the further propagation of the tear.

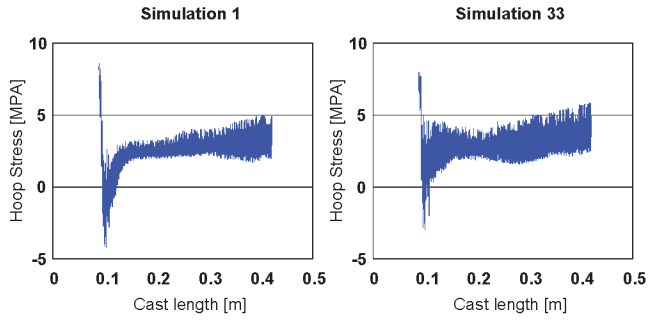


Figure 3: Hoop stress as a function of casting length for simulations 1 and 33, AA7108 alloy.

Comparison with the AA6060 alloy

A simulation of a casting of an AA6060 alloy with more or less standard Hydro casting parameters has been performed. The resulting hoop stresses are compared with the results of simulation no. 1 with the AA7108 alloy in Figure 4. Instead of the clear maximum and minimum stresses at the starting period, some oscillations in the hoop stress are observed. At the start-up phase of the casting the tensile stress of the AA6060 casting reaches the values of the AA7108 alloy. After less than 0.2 m of the casting the hoop stress at the surface of the AA6060 alloy reaches a stable level around 0 MPa. This is consistent with observations of AA6060 extrusion ingots that may have a short initial crack at the start of the casting. The major difference between these alloys is the last part of the solidification path. Both alloys start to solidify around 650°C, but the AA7108 alloy is not completely solidified before around 410°C. At a solid fraction of 0.975, the corresponding temperature for the AA6060 alloy is around 600°C and for the AA7108 alloy it is around 470°C. This means that the AA7108 alloy experiences a much higher stress and strain rate in the critical range as the $f_s$=0.975 isotherm comes much closer to the water hit region than for the AA6060 alloy. This is illustrated in Figures 5 to 9, where the hoop stress fields and the temperature fields are plotted for the steady state regime for the two cases.

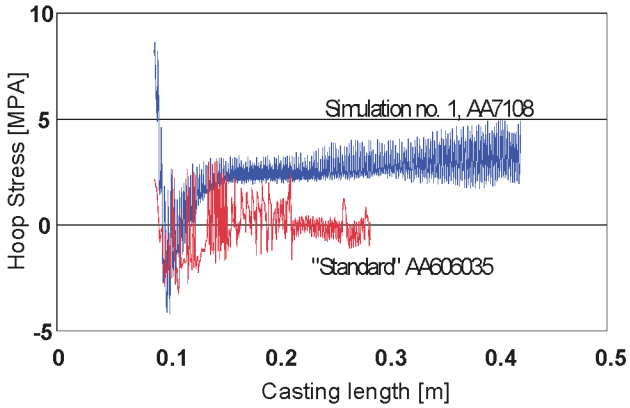


Figure 4: Hoop stress as a function of casting length for simulation no. 1 and a "standard" simulation of a casting with an AA6060 alloy (203 mm diameter).

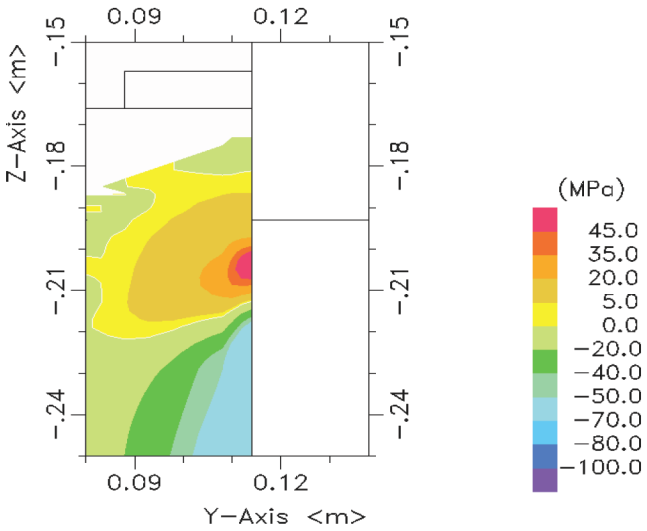


Figure 5: Hoop stress field for the surface region in the steady state regime for the AA6060 alloy. The mould ends at approx. 0.193 m.

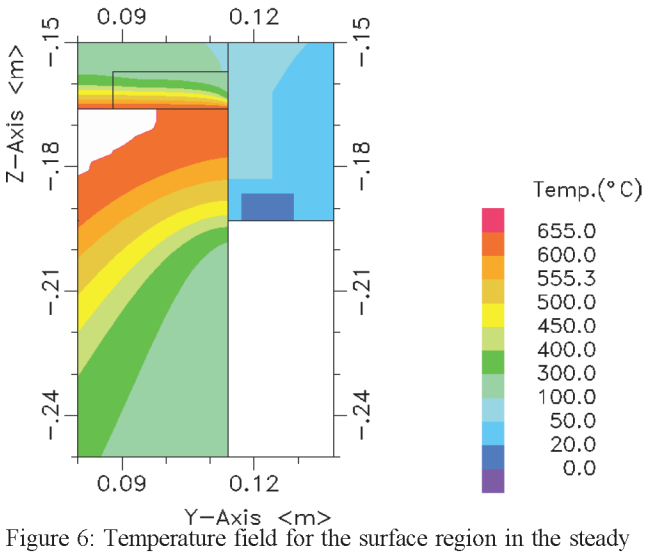


Figure 6: Temperature field for the surface region in the steady state regime for the AA6060 alloy. The mould ends at approx. .193 m. and the solidus temperature is around 555°C.

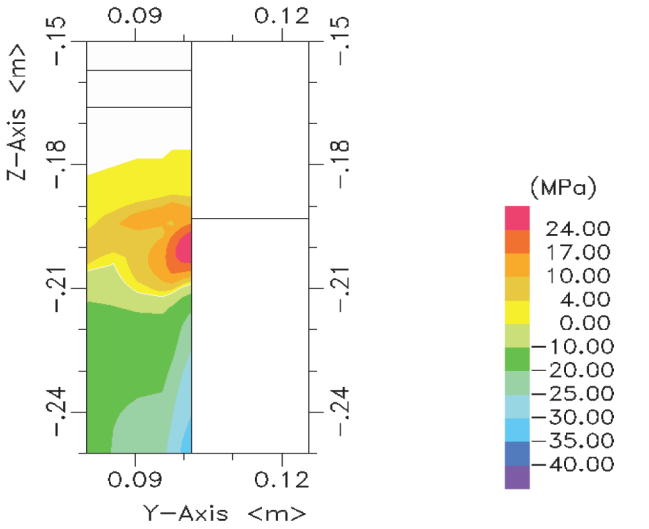


Figure 7: Hoop stress field for the surface region in the steady state regime for the AA7108 alloy. The mould ends at approx. 0.193 m.

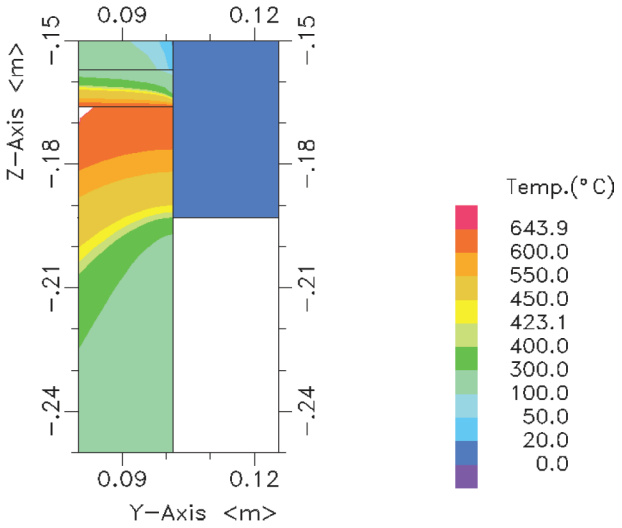


Figure 8: Temperature field for the surface region in the steady state regime for the AA7108 alloy. The mould ends at approx. 0.193 m and the solidus temperature is around 423°C.

Statistical analysis of the modelling results

Linear regression was performed including all parameters (coded values) and their combinations with respect to the maximum hoop stress, $\sigma_{max}$, the minimum hoop stress, $\sigma_{min}$, and the steady state hoop stress, $\sigma_{cont}$. The parameters where then plotted in normal distribution plots that are shown in Figures 9-11. Based on these plots it seems as if the linear models yield a "noise" interval from -0.1 to 0.1. Coefficients larger than an absolute value of 0.1 are therefore probably significant signals. Values from 0.07 to 0.1 represent here a grey area. The parameters that were found to yield a significant signal for the different response parameters are marked with pink (squares) and labelled.

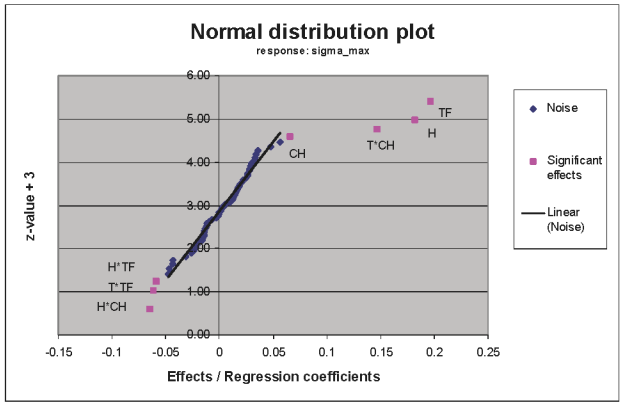


Figure 9: Normal distribution plot for $\sigma_{max}$ .

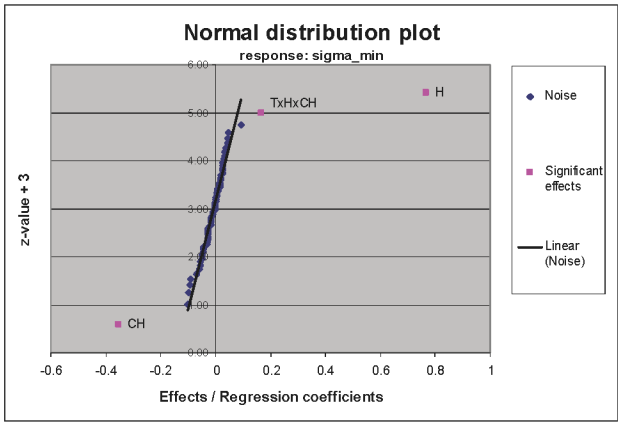


Figure 10: Normal distribution plot for $\sigma_{min}$ .

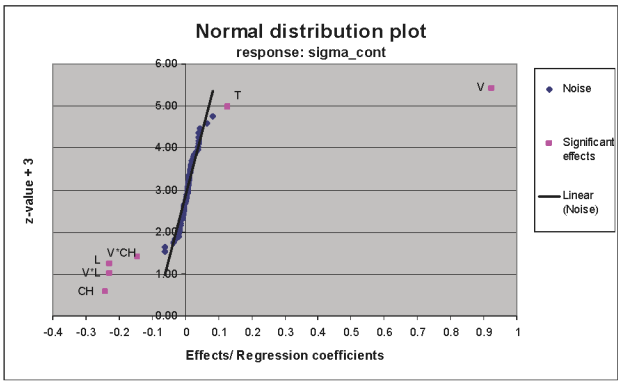


Figure 11: Normal distribution plot for $\sigma_{cont}$.

Linear regressions were then performed only with the parameters (real values) yielding a significant signal. The resulting coefficients with statistics are given in Table II. The linear models were used to calculate the effect of changing the most influential main variable. In the calculations the other significant variables were kept at a high (+1) and low value (-1). The resulting hoop stresses are shown in Figures 12-14 with indicated validity ranges of the variables. Note that within the validity ranges the maximum stress is minimised by choosing the lowest values (Min. Var.) of the other parameters, whilst the lowest values for the minimum and steady state stresses are achieved by choosing the highest values of the other variables (Max. Var).

To investigate this further, the hoop stresses have been maximised and minimised within the valid variable range. The resulting stresses are given in Table III together with the variables. The results show that it is beneficial to reduce the cone height, increase the initial metal temperature and reduce the effect of water cooling in order to reduce the maximum hoop stress. The minimum stress is reduced by decreasing the cone height and by increasing the cooling height and the casting temperature. The steady state stress is reduced primarily by reducing the casting speed, but also a reduction in the metal temperature, an increased cooling height and an increased ramping length are beneficial.

Table II Significant linear regression coefficients and constants for the DOE simulations (real values). All numbers relate to MPa and the denotations given in Table I

| Response | $\sigma_{max}$ | Const. | 6.3 | Std. Error of Estimate | | 0.2 | $R^2$ | 0.75 |
|---|---|---|---|---|---|---|---|---|
| Variable | $T_F$ | CH | H | $TxT_F$ | TxCH | | $HxT_F$ | HxCH |
| Coeff. | 0.036 | -0.21 | 31 | -4.8E-5 | 33E-5 | | -0.037 | -0.29 |
| Std.error | 0.006 | 0.04 | 6.6 | 8E-6 | 6E-5 | | 0.015 | 0.11 |
| Response | $\sigma_{min}$ | Const. | -3.9 | Std. Error of Estimate | | 0.35 | $R^2$ | 0.86 |
| Variable | | H | | CH | | TxHxCH | | |
| Coeff. | | 51.6 | | -0.026 | | -6E-4 | | |
| Std.error | | 7.9 | | 0.006 | | 3E4 | | |
| Response | $\sigma_{cont}$ | Const. | -3.2 | Std. Error of Estimate | | 0.24 | $R^2$ | 0.95 |
| Variable | V | L | T | CH | VxL | | VxCH | |
| Coeff. | 3998 | 2.2 | 0.003 | 0.020 | -2396 | | -31.8 | |
| Std.error | 281 | 0.45 | 0.001 | 0.009 | 308 | | 6.5 | |

Table III Maximum and minimum stresses for the three different stages of hoop stresses occurring during casting of the AA7108 alloy calculated from the linear model given in Table II

| **Stress [MPa]** | | **Variable** | V [m/s] | L [m] | T [°C] | $T_F$ [°C] | CH [mm] | H [m] |
|---|---|---|---|---|---|---|---|---|
| $\sigma_{max}$ | Max | 8.6057 | | | 650 | 375 | 30 | 0.044 |
| | Min | 7.461 | | | 710 | 225 | 30 | 0 |
| $\sigma_{min}$ | Max | -2.9244 | | | 650 | | 30 | 0.044 |
| | Min. | -5.2 | | | 710 | | 50 | 0 |
| $\sigma_{cont}$ | Max | 4.925746 | 0.00183 | 0.08 | 710 | | 30 | |
| | Min. | 1.9632 | 0.00092 | 0.5 | 650 | | 50 | |

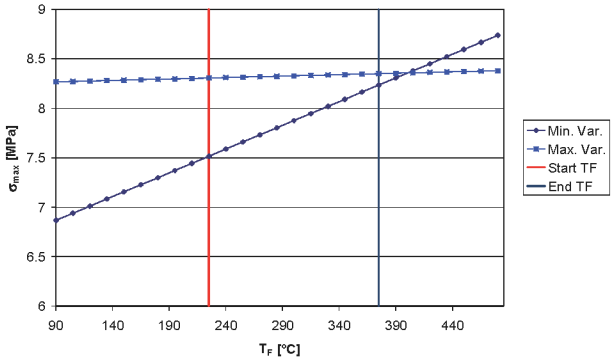


Figure 12: Hoop stress $\sigma_{max}$ calculated by utilising the linear model in Table II as a function of the film boiling temperature with high (+1) and low (-1) values of the other significant variables.

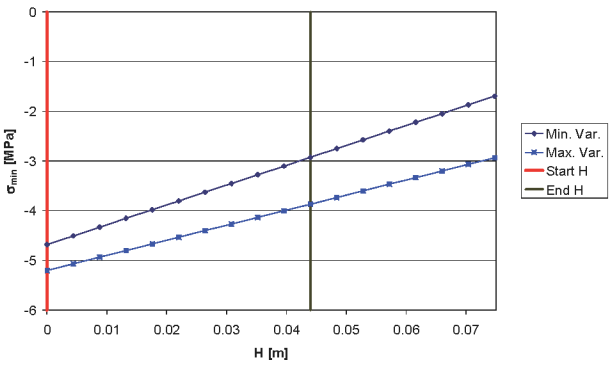


Figure 13: Hoop stress $\sigma_{min}$ calculated by utilising the linear model in Table II as a function of the cone height with high (+1) and low (-1) values of the other significant variables.

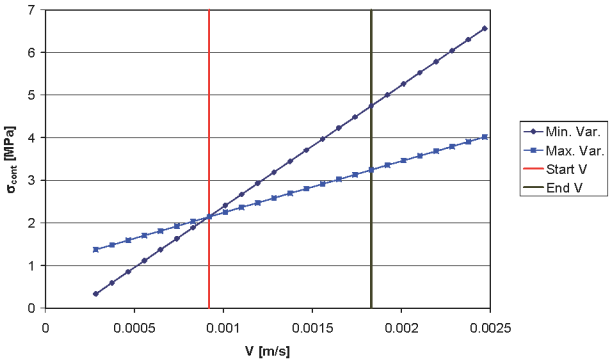


Figure 14: Hoop stress $\sigma_{cont}$ calculated by utilising the linear model in Table II as a function of the casting speed with high (+1) and low (-1) values of the other significant variables.

## Metallographic investigations

### Crack topography

A typical crack with the fracture surface are shown in Figure 15 and 16. The cracks penetrate 30-40 mm into the ingot and occur with relatively uneven distances. The fracture surface is grey and appears very oxidised. This is further investigated in the next paragraph. A closer view of the cracks shows that the cracks are fragmented, with several cracks surrounding the main crack. It seems as cracks having a direction deviating from the radial direction are stopped. This fragmentation of the cracks indicates that the cracks are intercrystalline. This is supported by a more thorough analysis of the fracture surface in Figure 15. Typically, a smooth surface topography is found with dendrite tips pointing into the fracture surface. This is illustrated by the image in Figure 16 that gives a closer view of the crack surface in Figure 15. In other parts of the crack there were observed large amounts of intermetallic particles. There were found no evidence of dendrite bridging, i.e., areas with deformed dendrites, at the surface.

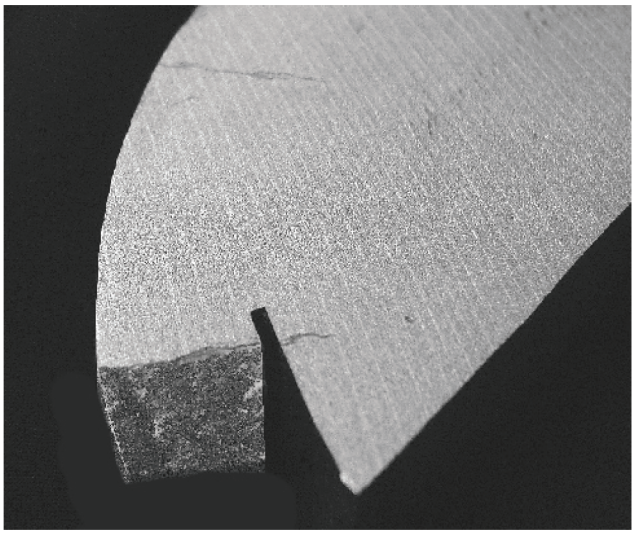

Figure 15: Part of and ingot slice with a fracture surface and one crack showing in the back of the image.

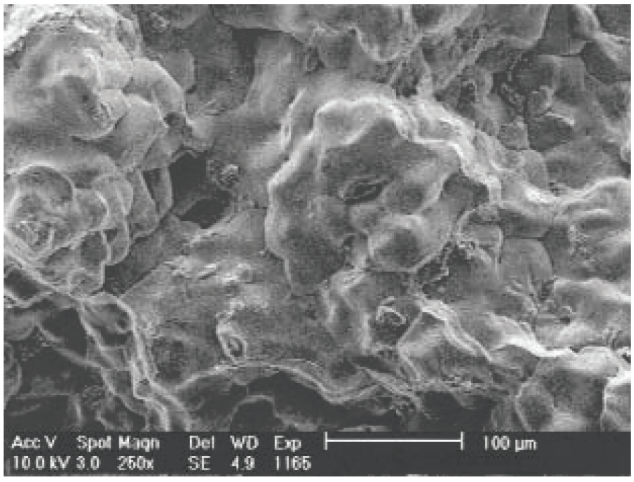


Figure 16: A typical part of the fracture shown in Figure 10 with dendrites pointing out of the surface.

### Crack surface analyses

As the fracture surface looked quite oxidised EDAX area analyses were performed at different positions from the surface. The results of the analyses are given in Figure 17. The analyses were performed with an acceleration voltage of 3.0 kV that gives a penetration depth of the electron beam around 0.1-0.2 µm . The main elements found were C, O, Zn, Mg and Al. Typically, at the outer crack surface a high concentration of C is found. The C content decreases into the ingot but is still around 10 wt.% 14 mm below the ingot surface. The O content is rather high through the whole surface, around 30 wt.%. This indicates that the surface of the fracture is heavily oxidised. At the outer fracture surface of the crack the amount of Zn is lower than then nominal content of Zn in the alloy, but approaches the nominal content and exceeds this further into the crack. The content of Zn is, however, lower than expected due to microsegregation during solidification. The Mg content at the fracture surface exceeds the nominal content by ten times at the outer crack and even more into the crack. The increased content of the alloying

elements at the cracked surface indicates that the crack has propagated between dendrites, i.e., the crack is intercrystalline.

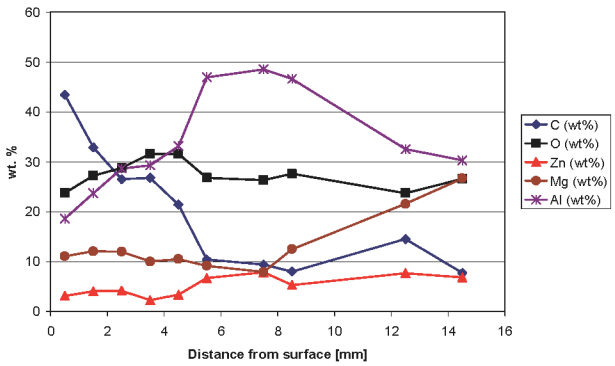


Figure 17: Results of EDAX analyses of crack surface areas at different positions from the surface of the ingot.

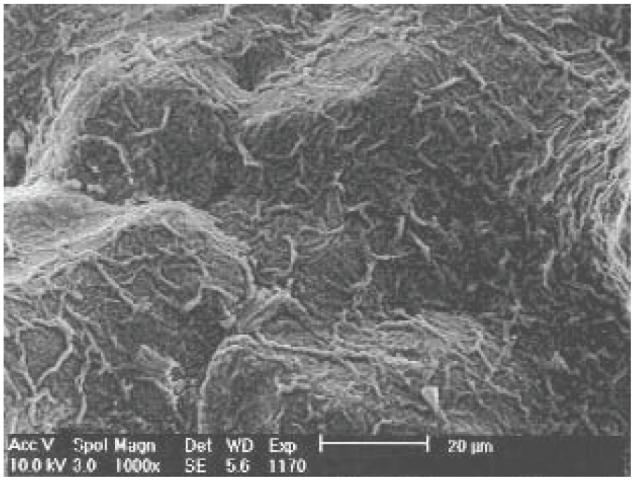


Figure 18: Fracture surface with oxide film.

The lubricating oil used during casting might have caused the large amount of C. This is consistent with the decreasing content of C into the crack. The high content of O at the fracture surface indicates that a thick surface oxide has formed on the surface during casting. The film is also easily observed on the fracture surface, see Figure 18. The oxide film consists probably of Mg and Al oxides. The oxides layer at the crack surface seems to be thicker and more developed than that found on the ingot surface. It is therefore believed that the film is formed at a high temperature and probably with liquid present and with enough O present. The formation of this oxide film and the role of it concerning the crack formation are discussed below.

## Discussion

Through modelling the general thermomechanical aspects of surface cracking during DC casting of an AA7108 alloy is revealed. Three main stages that influence the probability for cracks are identified. The surface region experiences first a maximum hoop stress that might open cracks. Secondly, a minimum hoop stress (pressure) occurs that might close a crack generated by the maximum stress. Then a steady state hoop stress is achieved at the steady state part of the casting. The effect of the main casting parameters are summarised in Tables II and III and it should be beneficial to adjust the casting parameters to have low stresses. The three stages are not found simulating the stresses occurring during casting of an AA6060 alloy and the steady state stress is very low for this alloy. The main difference here is the much broader solidification interval of the AA7108 alloy that moves the critical temperature region for cracking to an area with higher tensile stresses.

The above findings are, however, not enough to explain the fact that in a casting with several ingots only a few of the ingots may crack. I.e., even though the ingots experience more or less identical casting parameters some crack and some do not. It might be explained by mould variations in gas amount or metal temperature that may induce higher stresses for some ingots. However, it is also necessary to include the heterogeneities that exist prior to or form during casting. Observations of cracks initiating from oxide lumps on the surface may lead into an explanation. Oxide lump or clusters of oxide films will give heterogeneities in the material and act as crack initiators. Such inclusions are induced when poorly controlled moulds generate a lot of gas bubbling.

Another observation is the heavily oxidized fracture surface. Two explanations for this might be given. I) Oxidising as the crack opens might cause the film on the surface. Then, oxygen may be supplied by moist from the cooling water and air. This oxidizing, which is enhanced by the presence of Mg, may hinder the crack in closing. II) The oxide film formed on the surface of the gas pocket meniscus in the mould may be folded and dragged down into the ingot. This might happen due to sticking of the oxidised surface of the meniscus to the solidified metal during the start up phase or due to large gas bubbles in the hot top area pushing the oxide film towards the solidified metal. Also it might be due to larger oxide lumps dragged down from the top of the casting. There are three observations that indicate that the first explanation is the most valid one. Firstly, the fracture surface is more heavily oxidised than the surface of the casting, which actually is covered by the oxide film formed in the meniscus area [12]. Secondly, the cracks penetrate radial into the ingot. Physically, the meniscus is much more unstable and should give more changing directions of the crack. Thirdly, the crack do not close or change even though a string is used to stir the melt in the meniscus area [1]. In support of theory I is the high content of C at the fracture surface. The carbon has to come from the lubricating oil and this corresponds to a formation of the oxide in near contact with the mould wall or at the top of the oxide meniscus.

To conclude, both larger oxide lumps from the surface or clusters of oxide films generated by the gas slip system, are found to act as crack initiators. The role of the oxide film on the fracture surface is yet not fully understood, but it is believed that it makes it difficult for cracks to close and heal.

## Conclusions

The stress indicator used in the present work, the hoop stress at a solid fraction of 0.975, showed that the investigated AA7108 alloy performed quite different from an AA6060 alloy and was more susceptible to hot tearing at the ingot surface. Three important stages were identified that may explain the difference in crack behaviour. During the start up phase the hoop stress started at a maximum level, then dropped to a minimum level and reached a steady state level (tension) in the steady state

casting period. For the AA6060 alloy only some oscillations were found in the initial stage and then the stress levelled out around zero stress. The effect of casting parameters has been explored by a statistical approach and Tables II and III summarises the findings.

The cracks apparently being initiated at heterogeneities as oxide lumps and oxide films.

## Acknowledgement

The authors would like to thank the Hydro Aluminium Raufoss Automotive and the Norwegian Research Council for financing this work. Thanks are also due to Sverre Hanaset and Jan Sivertsen for practical information and Kolbjørn Halse for assistance with the statistics.

## References

1. J. Sivertsen, S. Hanaset, Unpublished work by Hydro Aluminium A.S. R&D Materials technology and Hycast A.S.

2. S. Benum, D. Mortensen, H.G. Fjær, "Prediction of boundary conditions and hot spots during the start-up phase of an extrusion ingot casting", in K. Ehrke and W. Schneider, editors, Continuous Casting, WILEY-VCH Verlag, (2000) pp.54-60.

3. D. Mortensen, "A mathematical model of the heat and fluid flows in direct-chill casting of aluminium sheet ingots and billets", Metall. and Materials Trans., 30B (1999), pp.119-133

4. H. G. Fjær and A. Mo, "ALSPEN - A Mathematical Model for Thermal Stresses in Direct Chill Casting of Aluminium Billets", Metall. Trans., 21B (1990), pp. 1049-1061.

5. H. G. Fjær, D. Mortensen, A. Håkonsen, E. A. Sørheim. "Coupled Stress, Thermal and Fluid Flow Modelling of the Start-up Phase of Aluminium Sheet Ingot Casting", Light Metals, TMS, Warrendale, PA, 1999, 743-748.

6. M. M'Hamdi, S. Benum, D. Mortensen, H.G. Fjær, J.-M. Drezet, "Experimental and numerical study of hot tearing formation during the start-up phase of a DC cast extrusion ingot", Submitted to Metallurgical and Materials Transactions, 2001.

7. C. L. Martin, D. Favier, and M Suéry, "Fracture behaviour in tension of viscoplastic porous metallic materials saturated with liquid", Int. Journal of Plasticity, 15 (1999), 981-1008.

8. Box G.E.P., Hunter W.G., Hunter J.S., Statistics for experimenters, John Wiley & Sons (1978), p.374.

9. Henriksen B.R, Braathen S.E., Jensen E.K., "The influence of casting practice on stresses and strains in 6xxx billets – A statistical and modelling study", in K. Ehrke and W. Schneider, editors, Continuous Casting, Wiley-VCH Verlag (2000), pp.185-190.

10. Dons A.L. & al., "The Alstruc microstructure solidification model for industrial aluminium alloys", Met. Trans. A, Vol. 30A (1999), pp. 2135-2146.

11. Fjær H, Mo A., "Alspen – a mathematical model for thermal stresses in DC casting of aluminium billets", Met. Trans.B, Vol.21B (1990), pp.1049-1061.

12. Ekenes M.E., Peterson K.W, "Visual observations inside and AIRSLIP™ mold during casting", Light Metals (1990), pp.957-961.